Beam test performance of the highly granular SiW-ECAL technological prototype for the ILC.

corresponding author

Abstract

High precision physics at future colliders as the International Linear Collider (ILC) require unprecedented high precision in the determination of the final state of the particles produced in the collissions The needed precision will be achieved thanks to the Particle Flow algorithms (PF) which require compact, highly granular and hermetic calorimeters systems. The Silicon-Tungsten Electromagnetic Calorimeter (SiW-ECAL) technological prototype design and R&D is tailored to the baseline design of the ECAL of the International Large Detector (ILD) for the ILC. In this document we present and discuss the commissioning of the prototype and the performance of the device in a beam test carried at DESY in June 2017.

Keywords: Calorimeter methods, calorimeters, Si and pad detectors

1. Introduction

Future accelerator based particle physics experiments require very precise and detailed reconstruction of the final states produced in the beam collisions. A particular example is the next generation of e^+e^- linear colliders such the ILC[1, 2, 3, 4, 5]. This project will provide collisions of polarized beams with centre-of-mass energies ($c.m.e$) of 250 GeV - 1 TeV. These collisions will be studied by two multipurpose detectors: the International Large Detector (ILD) and the Silicon Detector (SiD)[5]. To meet the precision levels required by the ILC physics goals, new techniques relying on single particle separation to make possible the choice of the best information available in the full detector to measure the energy of the final state objects have been developed. These techniques are called Particle Flow (PF) techniques [6, 7, 8] and allow to reduce the impact of the poor resolution of the calorimeter systems (compared with trackers) in the overall reconstruction. The detectors optimized for PF algorithms have some requirements. In the case of calorimeters: highly granular, compact and hermetic calorimeters. The CALICE collaboration is doing R&D of highly granular calorimeters [8] for future linear colliders.

In this document we will focus in the description of the silicon-tungsten electromagnetic calorimeter, SiW-ECAL, its commissioning and its performance in beam test. The SiW-ECAL is the baseline choice for the ILD ECAL. It consists in a detector (in the barrel region) of 24 X_0 of thickness which corresponds to $\sim$ 1 λ_I (interaction length). It has silicon (Si) as active material and tungsten (W) as absorber material. The combination of Si and W choices makes possible the design and construction of a very compact calorimeter with highly granular and compact active layers. It will consist of an alveolar structure of carbon fiber into which modules made of tungsten plates and the active sensors will be inserted. The very-front-end (VFE) electronics will be embedded in the SLABs. The silicon sensors will be segmented in squared cells (or channels) of 5x5 mm: a total of $\sim$ 100 million channels will constitute the ECAL for ILD. The desired signal dynamic range in each channel goes from 0.5 MIP to 3000 MIPs. To reduce overall power consumption, the SiW-ECAL will exploit the special bunch structure foreseen for the ILC: the e^+e^- bunchs trains will arrive within acquisition windows of $\sim$ 1-2 ms width separated by $\sim$ 200 ms. During the idle time, the bias currents of the electronics will be shut down. This technique is usually denominated power pulsing. In addition to this, to cope with the large amount of channels, the calorimeters should work in self-trigger mode (each channel featuring a discriminator for internal trigger decision) and zero suppression mode.

Email address: irles@lal.in2p3.fr (corresponding author)

2. The SiW-ECAL technological prototype

The first SiW-ECAL prototype was the so called SiW-ECAL physics prototype [9, 10, 11, 12, 13, 14]. It was successfully tested at DESY, FNAL and CERN running in front of another prototype from the CALICE collaboration, the analogue hadronic calorimeter AHCAL, delivering the proof of concept of the technollogy and the PF calorimetry. For the physics prototype, the VFE was placed outside the active area with no particular constraints in power consumption. It consisted of 30 layers of Si as active material alternated with tungsten plates as absorber material adding a total of 24 X_0. The active layers were made of a matrix of 3x3 Si wafers of 500 μm thickness. Each of these wafers was segmented in matrices of 6x6 squared channels of 1x1 cm^2, allowing for density of 1500 channels/dm^3 That very first prototype offered a signal over noise on the measured charge of 7.5 for MIP like particles.

The new generation prototype is called the SiW-ECAL technological prototype. It addresses the main technological challenges: compactness, power consumption reduction through power pulsing and VFE inside the detector close to real ILD conditions. It will also provide data to deeply study the PF and provide input to tune simulation programs as for example GEANT4[15, 16, 17] which is widely used in particle physics to simulate the passage of particles through matter.

The entity of sensors, thin PCB (printed circuit boards) and ASICs (application-specific integrated circuits) is called Active Signal Units or ASU. An individual ASU has a lateral dimension of 18x18 cm^2. The ASUs are currently equipped further with 16 SKIROC2[18, 19, 20] (Silicon pin Kalorimeter Integrated ReadOut Chip) ASICs for the read out and features 1024 square pads (64 per ASIC) of 5x5 mm. Each channel of the SKIROC is made of a variable-gain preamplifier followed by two two branches: a fast line for trigger decission and a slow line for dual-gain charge measurement. The charges stored in the buffers of a switched capacitor array are converted by a 12-bit Wilkinson ADC. The ASIC also features power pulsing that allow to reduce its consomation to 25 μW per channel. This feature is used for all data discussed in this paper and for first time in long periods of data taking in beam test. The channels and ASICs are distributed along the ASU as shown in Figure 1. Each ASU is equipped with 4 silicon wafers. The sensors consist on floating zone silicon wafers 320μm thick with high resistivity (bigger than 5000 Ω·cm). The size of the wafer is 9×9 cm^2 and it is subdivided in an array of 256 PIN diodes of 5×5 mm^2. A MIP (minimum ionizing particle) traversing the PIN parallel to its normal will create $\sim$ 80 h^+e^- pairs per μm which corresponds to 4.1 fC for particles incident perpendicularly to its surface. The high voltage is delivered to the wafers using a high voltage kapton sheet that covers the full extension of the wafers.

The readout layers of the SiW-ECAL consist of a chain of ASUs and an adapter board to a data acquisition system (DAQ) at the beginning of the layer. The readout layers are embedded on a "U" shape carbon structure to protect the wafers. The full system is then covered by two aluminum plates to provide electromagnetic shielding and mechanical stability. This ensemble is denominated SLAB ("short" for 1 ASU ensembles or "long" for ensembles of several ASUs enchained). With current SLABs design, a potential density of 3100 channels/dm^3 is achievable for the baseline ILD spatial constraints and X_0 requirements. This number should be compared with the density achieved in beam tests with the physics prototype: 1500 channels/dm^3. With the first versions of the technollogical prototype similar potential density level was reached but equipping only a quarter of the ASUs surface [19].

The SiW-ECAL detector designed for the ILD requires of the order of 10^5 highly integrated detection like the ones described in this text. For the production of the sample of SLABs studied in this document, a scalable working procedure has been established among several groups [21] profiting from the funding of projects like the AIDA2020 or the HIGHTEC emblematic project of the P2IO.

The subsequent chain of the data acquisition (DAQ) system [22] consists on three layers of modules. The first layer, or most downstream layer, consists on a set of detector interfaces called DIFs which are connected at the beginning of each SLAB to the ASUs via the adapter boards. They manage the communication with up to 15 ASUs. The second layer is made of concentrator card modules called the Gigabit Concentrator Cards (GDCCs) which are used to control up to 7 DIFs collecting all data from them and distributing among them the system clock and fast commands. The last layer consist on a clock and control card (CCC) which provides a clock, control fan-out of up to 8 GDCCs and accepts and distributes external signals (i.e. signals generated external pulse generator to simulate the ILC spill conditions). The whole system is controlled by the Calicoes and the Pyrame DAQ software version 3 [23, 24].

A photograph showing the SiW-ECAL technollogical prototype setup can be seen in Figure 2. Current prototype consists on 7 layers of SLABs housed by a PVC

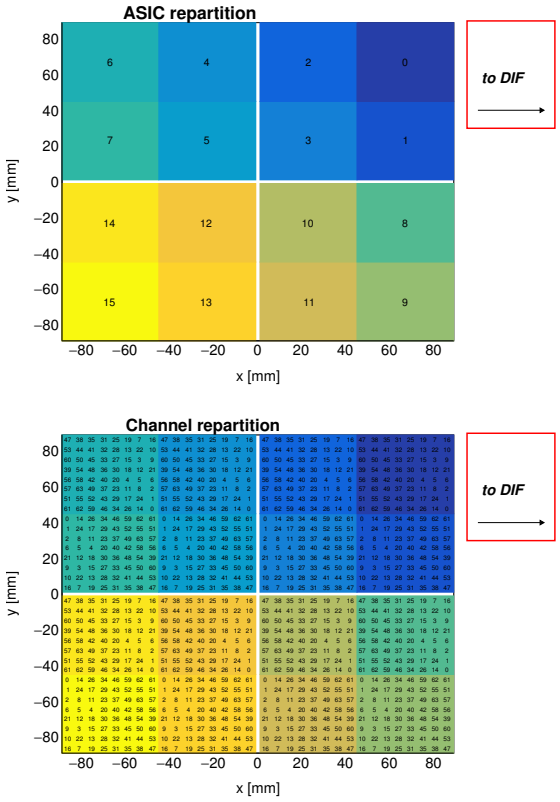

Figure 1: Repartition of the ASIC (up) and channels (down) in one ASU. In this perspective, the Si-Sensors are in glued in the back. The channels are separated (in x and y) by 5.5 mm. The empty cross in the middle of the ASU corresponds to the 1 mm separation between the sensors. The areas covered by the different ASICs and channels are labeled with numbers following design and DAQ criteria: from 0-16 in the case of the ASICs and from 0-63 in the case of the channels.

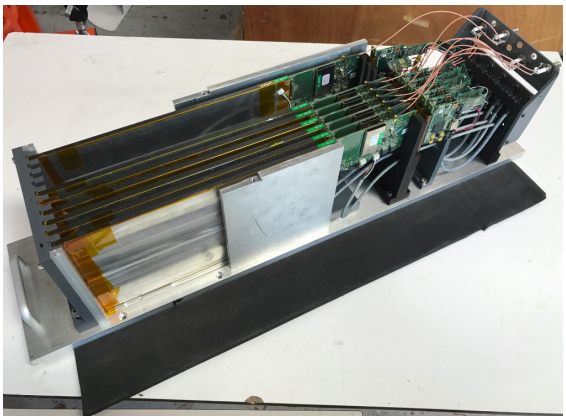

Figure 2: Prototype with 7 layers inside the aluminum stack.

and aluminum structure that can hold up to 10. For the beam test described in Section 3 all the layers were separated by equal distances of 15 mm except the last one which was at 60 mm of its nearest. In the following sections, we will refer to layers number 1 to 7, where the 1 is the closest to the beam pipe and 7 is the farthest. The detector was exposed to a positron beam in the DESY test beam area (line 24). During the full data taking period at the DESY beam test facility, the detector was running in power pulsing mode without any extra active cooling system. and means of an external pulse generator we defined the length of the acquisition window to be 3.7 ms at a frequency of 5 Hz.

3. Performance on positron beam test at DESY

The beam test line at DESY provides continuous positron beams in the energy range of 1 to 6 GeV with rates from few hundreds of Hz to few KHz with a maximum of $\sim$ 3 KHz for 2-3 GeV. The particles beam ies produced as follows: first, the electron/positron synchrotron DORIS II is used to produced a photon beam via bremsstralhung when interacting with a carbon fiber target; secondly, these photons are then converted to electron/positron pairs; and, finally, the beam energy is selected with dipole magnets and collimators. In addition, DESY gives acces to a bore 1 T solenoid, the PCMag.

The physics program of the beam test can be summarized in the following points:

1. Calibration without tungsten absorber using 3 GeV positrons acting as minimum ionizing particle (MIPs) directed to 81 position equally distributed over the modules.
2. Test in magnetic field up to 1 T using the PCMag. For this test a special PVC structure was designed and produced to support one single SLAB. The purpose of such test was twofold: first to prove that the DAQ, all electronic devices and the mechanical consistency of the SLAB itself are able to handle strong magnetic fields; second to check the quality of the data and the performance of the detector during the data taking when running in a magnetic field.
3. Response to electrons of different energies with fully equipped detector, i.e. sensitive parts *and* W absorber.

First reports on this beam test can be find in Refs. [25, 26]. In this paper we discuss in detail the results of the pedestal, noise and MIP calibration in Section 3.2. We also show the results on the pedestal and noise stability when running inside a magnetic field in Section **??**. The study of the perfomance of the detector for

electromagnetic shower events will be covered in future publications.

3.1. Commissioning of the detector

Earlier experiences with the SKIROC2 ASIC are reported in Refs. [19, 20]). Internal SKIROC2 parameters found in these references are adopted in the following except if the opposite is stated. For example, the gain value of 1.2pF for the preamplifier is used. With this gain, the SKIROC2 ensures a linearity better than 90% for 0.5-200 MIPs, which is enough for electromagnetic showers created by few GeV electrons or positrons.

The commissioning of the prototype for this beam test was focus in the control of the noise. Therefore, dedicated runs at the laboratory were taken in order to identify and mask the noisy channels. Two different kinds of noisy channels were found: the ones that are noisy on all SLABs and those which are only noisy in one or a few of them. Preliminary inspections of the PCB hints that the first group is associated to routing issues on the PCB and hereafter they are labelled like this. In addition, if a silicon wafer presented a problem (high leaking currents) or an ASIC was labelled as fulty (more than 70% of channels identified as noisy) the corresponding sectors of the SLAB were fully masked. The summary of this study is shown in Figure 3. These channels are removed from the data taking in all the studies shown from now on.

3.1.1. Trigger threshold optimization and S/N ratio in the trigger decission

The threshold of the auto-trigger is optimized to minimize the noise hits but maximizing at the same time the efficiency for measuring the signals associated to particles crossing the detector. For this purpose, dedicated scans of trigger threshold values with only noise signals or with injected signals of different sizes are done. In Figure 4 we see threshold scans curves curves obtained for several channels in a SKIROC testboard [**?**] in which a single SKIROC2 in BGA package is placed and signals of 1 MIP and 2 MIPs size are directly injected in the preamplifier (via a 3 pF capacitor located in the injection line as shown in Figure **??**). From this plot we can extract a S/N ratio of ∼12.8. Similar results are expected for fully equipped ASUS that are optimized to meet the detector requirement and to hold several ASICs at the same time. The final choice of the trigger threshold values for all ASICs is shown in Figure 5.

3.2. Response to MIP-acting positrons

The calibration runs have been used to calculate the pedestal distribution reference values and the noise levels (the width of the pedestal distrution) of each channel. In Figure 6 we show the signal and pedestal distribution of a single channel after subtracting the pedestal mean position. The results of the MIP calibration fit are shown in red (see Section 3.2.2 for more details) The pedestal distribution is shown only for the first SCA to keep the y-axis within a reasonable range. The signal distribution is integrated over all SCAs.

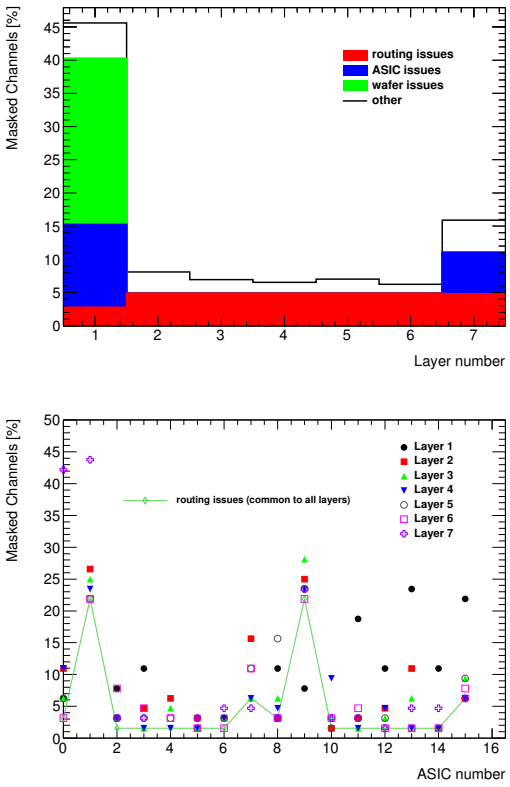

Figure 3: Ratio of channels that are marked as noisy in all slabs. Top: inventory of the different type of noisy channels per slab. Bottom: break down of the total number of noisy channels per ASIC. The ASICs 4-7 (wafer issue) and 10 from layer 1 and the ASIC 4 from layer 7 are not included in the second plot since they are fully masked.

3.2.1. Pedestal and noise determination

The pedestal is calculated as the mean position of the ADC distribution of channels without trigger. The noise is associated to the width of such distribution. The pedestal correction is done layer-, chip-, channel- and SCA-wisely due to the large spread of values between pedestals, as observed in Figure 7 (left plot) and Figure 8 (also left plot). For the noise, the dispersion is much smaller (∼ 5%). This is shown in the right plots of Figures 7 and 8. From now on, the pedestal correction is

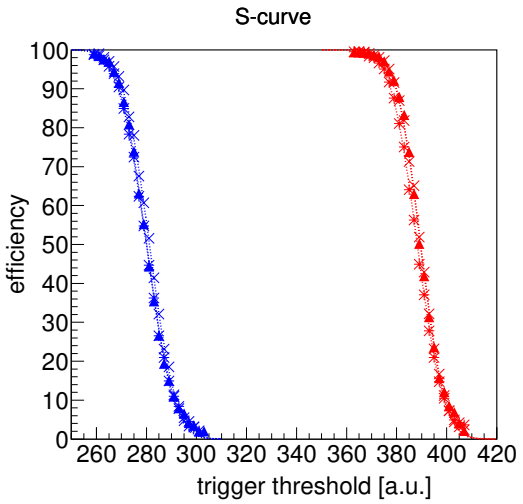

Figure 4: Threshold curves with charge injection (1 MIP in blue and 2 MIPs in red) for two different channels in a SKIROC2 testboard. From this plot, we extract a $S/N = 12.8$ in the trigger line.

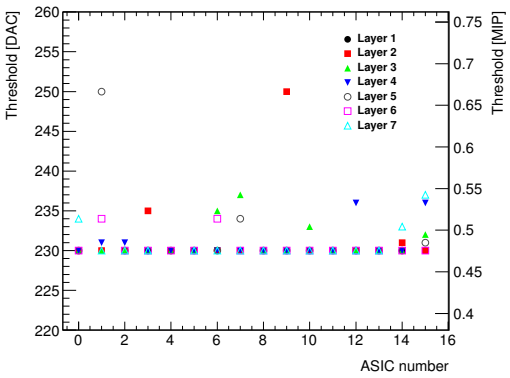

Figure 5: Summary of the trigger threshold settings in internal DAC units and in MIP units.

applied to all the results presented.

3.2.2. *Energy calibration and tracking efficiency*

After the pedestals are calculated and subtracted to the hit distributions, those are fit by a Landau function convoluted with a Gaussian. The most-probable-value of the convoluted function is taken as the MIP value, allowing thus for a direct conversion from ADC units to energy in MIP units. We have obtained a raw energy calibration spread of the 5% among all channels with the 98% of all available channels being fitted. Results are summarized in figure 9, leftmost plot.

We checked the MIP calibration in all callibrated channels by selecting tracks incident perpendicullary to the layers surface. The results are shown in figure 10

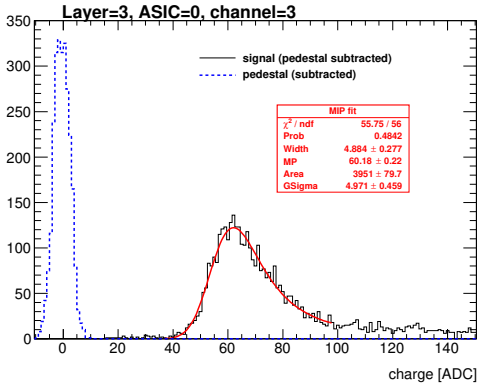

Figure 6: Pedestal (blue dashed line) and signal (black continuous line) distribution for one channel in the third layer.

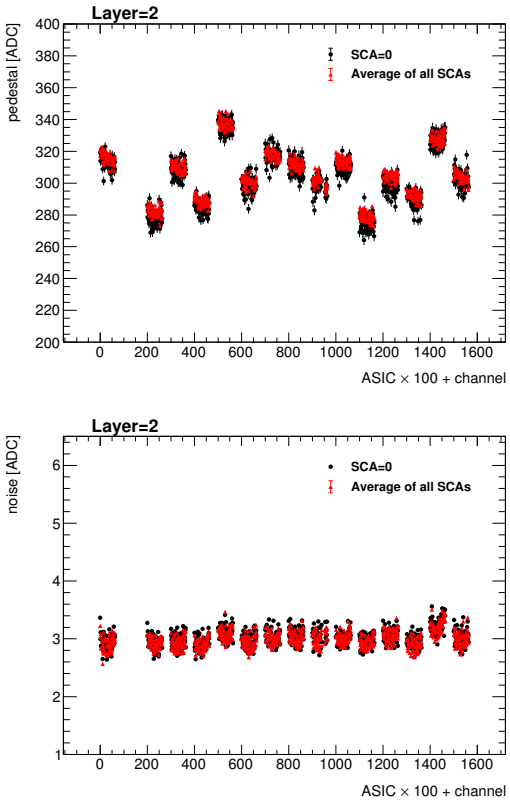

Figure 7: Pedestal mean position (upper plot) and width (lower plot) for all channels in one layer. The data is grouped on bunches in which the value in the x-axis corresponds to the value of the channel number plus the value of the ASIC number multiplied by 100. The black points show the value for the first SCA and the red points show the average value for all the others SCAs (with the standard deviation of the sample as error bar).

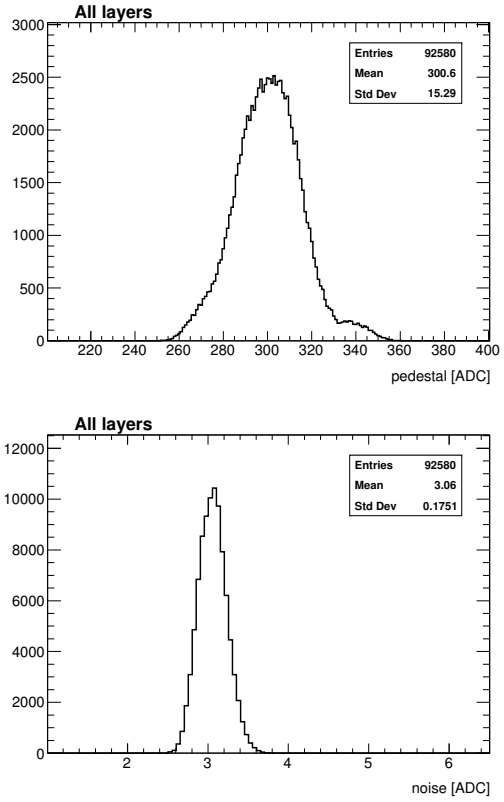

Figure 8: Pedestal mean position (upper) and width (lower) for all channels and all SCAs in the setup.

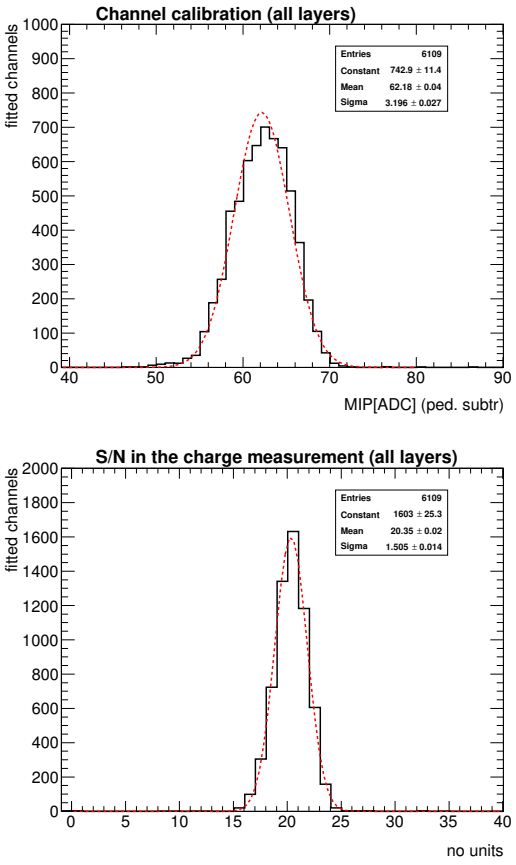

Figure 9: Result of the MIP calibration and signal over noise for the measured charge for all calibrated channels.

where the single channel energy distribution for MIPs is shown for all calibrated channels in the same distribution. The maximum peaks at 1 MIP as expected after a good calibration. In addition to this, a second and a third peak appear visible. These peaks are due to events involving multiple particles crossing the detector.

To evaluate the single hit detection efficiency we define a high purity sample of events by selecting tracks with at least 4 layers with a hit in exactly the same channel. Afterwards we check if the other layers have or not a hit in the same channel (expanding the search to the closest neighbouring channels) with energy larger or equal than 0.3 MIP. Finally, we repeat this for all layers and channels. The results are shown in Figure 11. Except few exceptions, the efficiency is compatible with 100%. Lower efficiencies in the first layer are related to the presence of noisy channels not spotted during the commissioning. In the last layer (separated from the other layers by four slots of 1.5 cm instead of only one) we also observe few small deviations from the $\sim$ 100% which are indeed associated to a slight misalignment of the detector. If we remove these channels from the analysis the full efficiency is recovered.

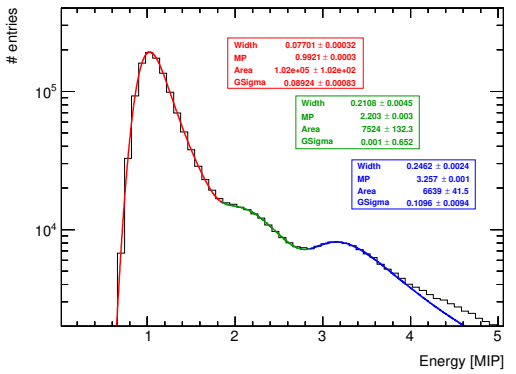

Figure 10: Energy distribution for all callibrated channels when selecting tracks of 3 GeV positron acting as MIPs.

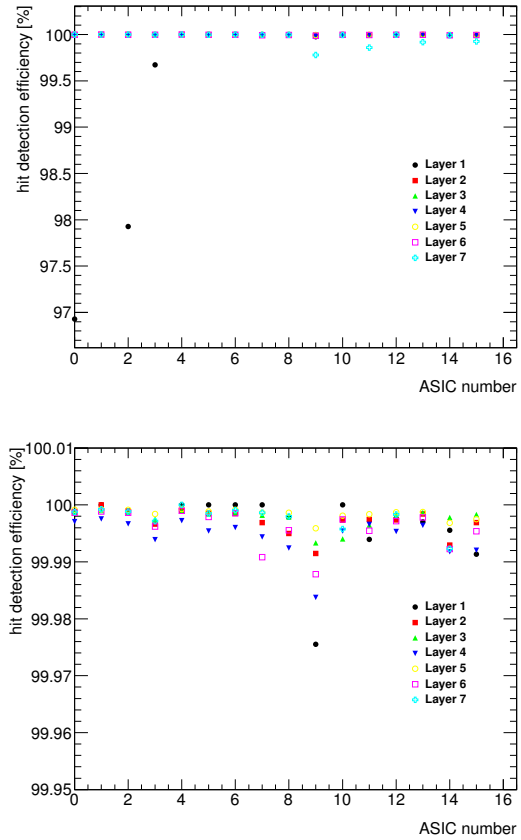

Figure 11: Upper plot: MIP detection efficiency for all layers and ASICs in high purity samples of tracks of MIP-like acting particles. Lower plot: same figures with a zoom in the y-axis. In both cases, the average efficiency of the 64 channels in each ASIC is shown.

3.2.3. S/N ratio in the charge measurement for MIP interactions

The signal-over-noise ratio in the charge measurement (corresponding to the slow shaper of the SKIROC2) is defined as the ratio between the most-probable-value of the Landau-gauss function fit to the data (pedestal subtracted) and the noise (the pedestal width). This quantity has been calculated for all channels and all layers. The average S/N is to 20.4. Results are summarized in Figure 9, lower plot.

3.3. Pedestal and noise stability in a magnetic field

The data taking inside the magnetic field has been divided in three steps: a) a with a magnetic field of 1 T; b) a run with 0.5 T; c) a final run with the magnet off. The beam, 3 GeV positrons, was hitting in the area of the PCB readout by the ASIC number 12.

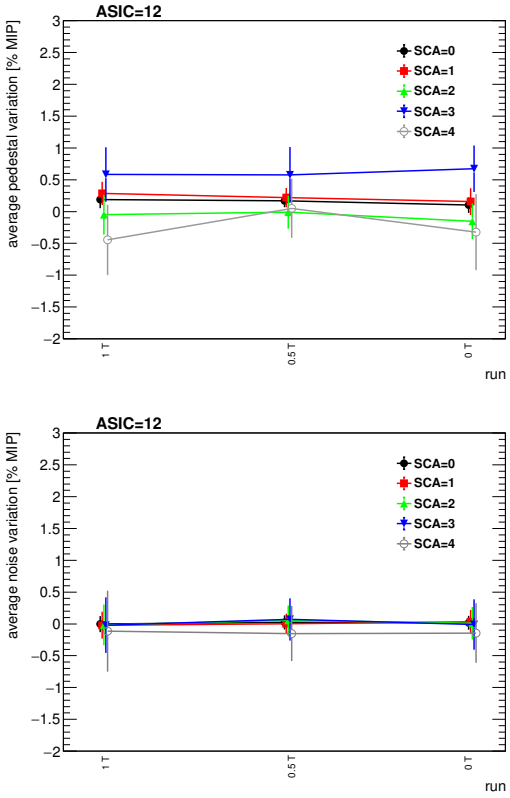

Figure 12: Average deviation of the pedestal mean position (left) and width (right) for all channels in the ASIC 12.

The pedestal positions and noise levels of the channels of the ASIC 12 when the SLAB is inside of the PCMag are compared with the results from the calibration run described in the previous section. This is shown in Figure 12. We see that the agreement is perfect within the statistical uncertainties. Due to the lower rates in this beam area, the analysis is only done up to few SCAs.

4. Summary and outlook

The R&D program of the highly granular SiW-ECAL detector is in an exciting phase. After the proof of principle of the imaging calorimetry concept using the physics prototype, the technological prototype is being constructed and tested. In this document we describe the commissioning and beam test performance of a prototype built in with the first fully assembled detector elements, in contrast with previous beam tests. In addition, with the setup used in this beam test we reached levels of granularity similar to the targets of the ILD detector for the ILC. This is also the first time that a SiW-ECAL prototype continuously takes data in a beam test running

in power pulsing mode, one of the crucial features for the detectors for the ILC. Finally, we tested the performance of the detector modules working for long periods inside magnetic fields.

A very comprehensive and detailed commissioning procedure has been established and optimized allowing us to identify and isolate the different noise sources that could spoil the data taking. The beam test has provided a lot of useful data to study the performance of the detector and to perform a channel by channel calibration, showing a good homogenity with a spread of the 5% for all channels. The signal over noise of the detector has been evaluated to be 12.8 for the trigger decission and 20.4 for the charge measurement using, in both cases, MIP signals as reference.

acknowledgments

This project has received funding from the European Union's Horizon 2020 Research and Innovation program under Grant Agreement no. 654168. This work was supported by the P2IO LabEx (ANR-10-LABX-0038), excellence project HIGHTEC, in the framework 'Investissements d'Avenir' (ANR-11-IDEX-0003-01) managed by the French National Research Agency (ANR). The research leading to these results has received funding from the People Programme (Marie Curie Actions) of the European Union's Seventh Framework Programme (FP7/2007-2013) under REA grant agreement, PCOFUND-GA-2013-609102, through the PRESTIGE programme coordinated by Campus France. The measurements leading to these results have been performed at the Test Beam Facility at DESY Hamburg (Germany), a member of the Helmholtz Association (HGF).

[1] T. Behnke, J. E. Brau, B. Foster, J. Fuster, M. Harrison, J. M. Paterson, M. Peskin, M. Stanitzki, N. Walker, H. Yamamoto, The International Linear Collider Technical Design Report - Volume 1: Executive SummaryarXiv:1306.6327.

[2] H. Baer, T. Barklow, K. Fujii, Y. Gao, A. Hoang, S. Kanemura, J. List, H. E. Logan, A. Nomerotski, M. Perelstein, et al., The International Linear Collider Technical Design Report - Volume 2: PhysicsarXiv:1306.6352.

[3] C. Adolphsen, M. Barone, B. Barish, K. Buesser, P. Burrows, J. Carwardine, J. Clark, H. Mainaud Durand, G. Dugan, E. Elsen, et al., The International Linear Collider Technical Design Report - Volume 3.I: Accelerator & in the Technical Design PhasearXiv:1306.6353.

[4] C. Adolphsen, M. Barone, B. Barish, K. Buesser, P. Burrows, J. Carwardine, J. Clark, H. Mainaud Durand, G. Dugan, E. Elsen, et al., The International Linear Collider Technical Design Report - Volume 3.II: Accelerator Baseline DesignarXiv:1306.6328.

[5] H. Abramowicz, et al., The International Linear Collider Technical Design Report - Volume 4: DetectorsarXiv:1306.6329.

[6] J.-C. Brient, H. Videau, The Calorimetry at the future e+ e- linear collider, eConf C010630 (2001) E3047. arXiv:hep-ex/0202004.

[7] V. Morgunov, A. Raspereza, Novel 3-D clustering algorithm and two particle separation with tile HCAL, in: Linear colliders. Proceedings, International Conference, LCWS 2004, Paris, France, April 19-23, 2004, 2004, pp. 431–436. arXiv:physics/0412108.
URL http://inspirehep.net/record/667651/files/arXiv:physics_0412

[8] F. Sefkow, A. White, K. Kawagoe, R. Pöschl, J. Repond, Experimental Tests of Particle Flow Calorimetry, Rev. Mod. Phys. 88 (2016) 015003. arXiv:1507.05893, doi:10.1103/RevModPhys.88.015003.

[9] C. Adloff, J. Blaha, J. J. Blaising, C. Drancourt, A. Espargiliere, R. Galione, N. Geffroy, Y. Karyotakis, J. Prast, G. Vouters, Tests of a particle flow algorithm with CALICE test beam data, JINST 6 (2011) P07005. arXiv:1105.3417, doi:10.1088/1748-0221/6/07/P07005.

[10] J. Repond, et al., Design and Electronics Commissioning of the Physics Prototype of a Si-W Electromagnetic Calorimeter for the International Linear Collider, JINST 3 (2008) P08001. arXiv:0805.4833, doi:10.1088/1748-0221/3/08/P08001.

[11] C. Adloff, et al., Response of the CALICE Si-W electromagnetic calorimeter physics prototype to electrons, Nucl. Instrum. Meth. A608 (2009) 372–383. arXiv:0811.2354, doi:10.1016/j.nima.2009.07.026.

[12] C. Adloff, et al., Study of the interactions of pions in the CALICE silicon-tungsten calorimeter prototype, JINST 5 (2010) P05007. arXiv:1004.4996, doi:10.1088/1748-0221/5/05/P05007.

[13] C. Adloff, et al., Effects of high-energy particle showers on the embedded front-end electronics of an electromagnetic calorimeter for a future lepton collider, Nucl. Instrum. Meth. A654 (2011) 97–109. arXiv:1102.3454, doi:10.1016/j.nima.2011.06.056.

[14] B. Bilki, et al., Testing hadronic interaction models using a highly granular silicon–tungsten calorimeter, Nucl. Instrum. Meth. A794 (2015) 240–254. arXiv:1411.7215, doi:10.1016/j.nima.2015.05.009.

[15] S. Agostinelli, et al., GEANT4: A Simulation toolkit, Nucl. Instrum. Meth. A506 (2003) 250–303. doi:10.1016/S0168-9002(03)01368-8.

[16] J. Allison, et al., Geant4 developments and applications, IEEE Trans. Nucl. Sci. 53 (2006) 270. doi:10.1109/TNS.2006.869826.

[17] J. Allison, et al., Recent developments in $G_{EANT}4$, Nucl. Instrum. Meth. A835 (2016) 186–225. doi:10.1016/j.nima.2016.06.125.

[18] S. Callier, F. Dulucq, C. de La Taille, G. Martin-Chassard, N. Seguin-Moreau, SKIROC2, front end chip designed to readout the Electromagnetic CALorimeter at the ILC, JINST 6 (2011) C12040. doi:10.1088/1748-0221/6/12/C12040.

[19] M. S. Amjad, et al., Beam test performance of the SKIROC2 ASIC, Nucl. Instrum. Meth. A778 (2015) 78–84. doi:10.1016/j.nima.2014.12.011.

[20] T. Suehara, et al., Performance study of SKIROC2/A ASIC for ILD Si-W ECAL, JINST 13 (03) (2018) C03015. arXiv:1801.02024, doi:10.1088/1748-0221/13/03/C03015.

[21] V. Boudry, R. Cornat, D. Lacour, R. Pöschl, F. Magniette, Advanced assembly chain for Si calorimeters.
URL http://cds.cern.ch/record/2318814

[22] F. Gastaldi, R. Cornat, F. Magniette, V. Boudry, A scalable gigabit data acquisition system for calorimeters for linear collider, PoS TIPP2014 (2014) 193.

[23] M. Rubio-Roy, F. Thiant, F. Magniette, Flexible online moni-

toring for high-energy physics with Pyrame, J. Phys. Conf. Ser. 898 (3) (2017) 032009. doi:10.1088/1742-6596/898/3/032009.

[24] F. Magniette, A. Irles, Pyrame 3, an online framework for Calice SiW-Ecal, JINST 13 (03) (2018) C03009. doi:10.1088/1748-0221/13/03/C03009.

[25] A. Irles, Latest R&D news and beam test performance of the highly granular SiW-ECAL technological prototype for the ILC, JINST 13 (02) (2018) C02038. arXiv:1802.08806, doi:10.1088/1748-0221/13/02/C02038.

[26] A. Irles, Latest developments on the highly granular Silicon-Tungsten Electromagnetic Calorimeter technological prototype for the International Large Detector, in: 2017 IEEE Nuclear Science Symposium and Medical Imaging Conference (NSS/MIC 2017) Atlanta, Georgia, USA, October 21-28, 2017, 2018. arXiv:1801.10407.
URL http://inspirehep.net/record/1651519/files/arXiv:1801.10407.pdf